

# Regulating Solvation Shell to Fortify Anion–Cation Coordination for Enhanced Sodium Metal Battery Stability

Zhangbin Cheng, Zehui Zhang, Feilong Qiu, Zheng Gao, Haijiao Xie, Zhen Xu, Min Jia,\*  
Xiaoyu Zhang,\* and Haoshen Zhou\*



Cite This: *ACS Energy Lett.* 2025, 10, 177–184



Read Online

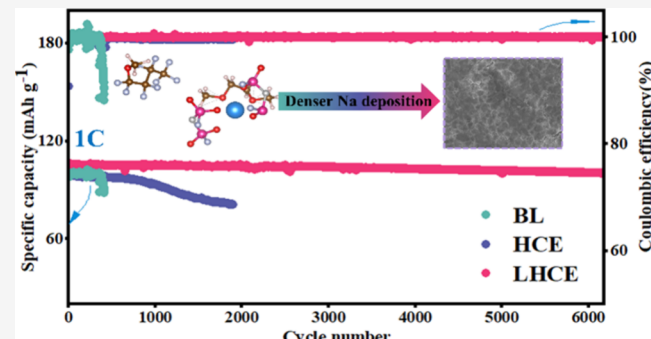
ACCESS |

Metrics & More

Article Recommendations

Supporting Information

**ABSTRACT:** The use of sodium metal as an anode presents a promising avenue for high energy density sodium rechargeable batteries given its high specific capacity and low redox potential. However, sodium metal batteries (SMBs) encounter significant challenges, including interfacial parasitic reactions and dendrite growth. Developing a robust solid electrolyte interphase (SEI) is crucial for SMB engineering. This study introduces hydrofluoroether as a diluent in high-concentration electrolytes, effectively modifying the solvation structure to enhance ion-pair coordination, which leads to an inorganic-rich SEI, mitigating sodium depletion and dendrite formation. Consequently, localized high concentration electrolytes achieve a 98.3% Coulombic efficiency in Na||Cu batteries, while the Na||NaFe<sub>1/3</sub>Ni<sub>1/3</sub>Mn<sub>1/3</sub>O<sub>2</sub> battery retains 86.4% capacity after 750 cycles at 1C. Additionally, the Na||Na<sub>3</sub>V<sub>2</sub>(PO<sub>4</sub>)<sub>3</sub> battery achieves an exceptional average Coulombic efficiency of 99.97% at 1C, with a capacity retention of 95.4% after 517 days. This study provides a framework for enhancing efficiency and longevity in SMBs that can be applied to other battery systems.



Sodium (Na)-ion batteries (SIBs) are considered as a new generation of energy storage systems with promising applications, owing to the plentiful sodium reserves and extensive availability.<sup>1,2</sup> Yet, the energy density of currently commercialized SIBs with hard carbon as the anode still have a relatively lower energy density compared with the Li-ion batteries. Compared to hard carbon and other Na insertion compounds (such as Na<sub>4</sub>Sn) with high costs and lower capacities, metallic Na is regarded as an attractive anode for the next-generation sodium metal battery (SMB) systems because of its low redox potential (−2.71 V vs standard hydrogen electrode) and high theoretical capacity (1165 mAh g<sup>−1</sup>). Therefore, the comprehensive study of the SMBs have garnered significant interest recently.<sup>3–5</sup> Utilizing metallic sodium as the anode in batteries presents a significant problem due to the intense chemical interaction with the electrolyte during the charge and discharge cycles.<sup>6,7</sup> This reaction not only poses a risk of safety incidents but also results in gradual depletion of the sodium anode material. Moreover, the creation of a labile solid electrolyte interphase (SEI) and the unregulated growth of sodium dendritic formations during this process lead to a low Coulombic efficiency and a compromised

cycling performance which severely hinder the application of the SMBs.<sup>8,9</sup>

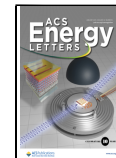
To address this problem, numerous strategies have been proposed, among which modifying the electrolyte to construct a stable SEI to repress the proliferation of sodium dendritic formations is one of the most convenient and effective methods.<sup>10,11</sup> Previously, the electrolyte studies concentrated on ether-based compounds, including 1,2-dimethoxyethane (DME), and matched sodium salts, including sodium bis-(fluorosulfonyl)imide (NaFSI). Due to the superior electrochemical stability of ethers with sodium metal, they are favored over the ester-based species commonly found in sodium metal batteries.<sup>12–15</sup> However, in such electrolytes, the quantity of solvents far exceeds that of anions, hence solvent molecules dominate the solvation structure of Na<sup>+</sup>, and a substantial

Received: October 5, 2024

Revised: November 8, 2024

Accepted: December 11, 2024

Published: December 16, 2024



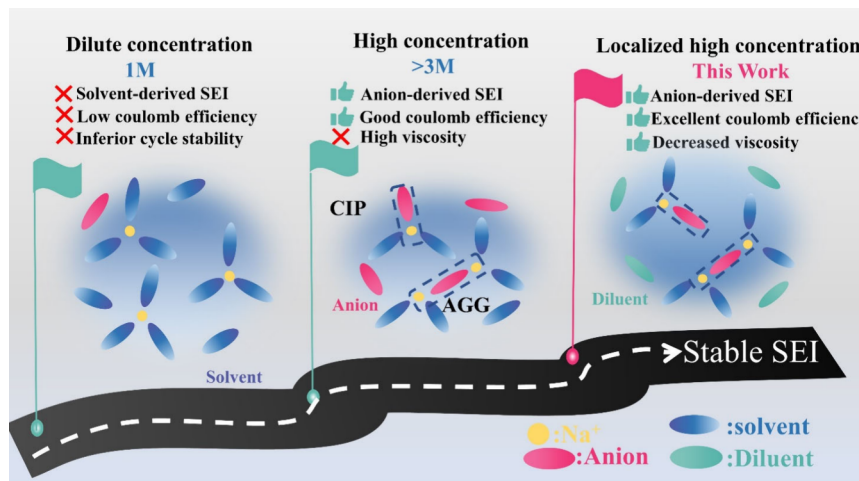


Figure 1. Diagram of the solvation configurations of  $\text{Na}^+$  in different electrolytes and their impact on the sodium metal battery.

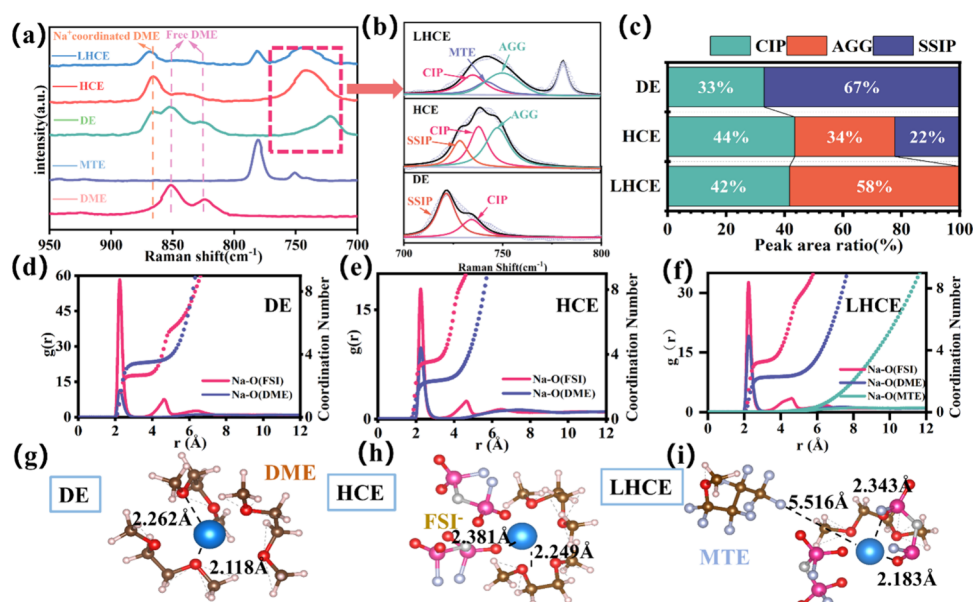


Figure 2. (a) Raman spectroscopic analysis for DE, HCE, and LHCE, alongside DME and MTE. (b) Raman spectroscopic data of the  $\text{FSI}^-$  anion in coordination, observed within the  $700\text{--}800\text{ cm}^{-1}$  frequency range. (c) In DE, HCE, and LHCE, the proportions of SSIP, CIP, and AGG structures are determined by the relative areas of the peaks observed in the Raman spectra. (d–f) MD simulations yield the radial distribution functions (solid lines) for  $\text{Na}-\text{O}(\text{DME})$ ,  $\text{Na}-\text{O}(\text{FSI})$ , and  $\text{Na}-\text{O}(\text{MTE})$  pairs alongside their coordination numbers (dotted lines) in electrolytes DE, HCE, and LHCE. MD simulation results in DE, HCE, and LHCE illustrate the interaction of  $\text{Na}^+$  with  $\text{FSI}^-$  and solvents DME or MTE as shown in (g–i), respectively.

presence of unbound solvent molecules is observed in the solution. A reaction between these solvent molecules and the metallic Na anode generated an SEI layer that was nonuniform, fragile, and characterized by slow interfacial kinetics, failing to effectively protect the Na metal anode. The undesired reactions between the sodium anode and electrolytes lead to a rapid decrease in the capacity drop in SMBs. Moreover, the unstable deposition of Na metal could easily lead to the formation of dead Na and dendrite growth. Persistent dendrite growth gave rise to battery short-circuits and severe exothermic reactions, potentially leading to electrolyte combustion and battery explosion.<sup>16,17</sup>

To establish a more reliable and durable anion-derived SEI, it is crucial to involve more anions in the solvation structure and reduce the quantity of free solvent molecules.<sup>18,19</sup> The use of weak solvating electrolytes (WSEs) has recently gained

widespread attention. In WSEs, solvents with “weak solvation power” interact weakly with  $\text{Na}^+$ , thus enabling more anions to pair with  $\text{Na}^+$ , forming abundant contact ion pairs (CIPs) and aggregate solvates (AGGs). Under such conditions, the electrode’s anodic stability is significantly improved. However, such solvents cannot fully dissociate sodium salts, and the poor salt dissociation leads to low ionic conductivity of the electrolyte. High-concentration electrolytes (HCEs) have drawn considerable notice due to their novel solvation design.<sup>20,21</sup> The increase in the salt concentration enriches the electrolyte with CIP and AGG solvation forms. This enables the creation of a stable anion-derived SEI under the drive of HCE, which compared to the solvent-derived SEI in traditional electrolytes is beneficial for  $\text{Na}^+$  transport and possesses better chemical stability and mechanical strength. This strategy successfully maintains the integrity of the

electrode surface, reduces volume changes and structural damage during charge–discharge processes, and effectively improves the plating/stripping Coulombic efficiency (CE) between metallic sodium and electrolytes.<sup>22,23</sup>

Zhang et al. designed a high-concentration electrolyte of 4 M NaFSI in dimethoxyethane (DME) to inhibit the proliferation of sodium dendrites and ensure high Coulombic efficiency in Na||Cu batteries and enable SMBs structured around the Na||Na<sub>3</sub>V<sub>2</sub>(PO<sub>4</sub>)<sub>3</sub> framework to operate at high rates and high efficiency.<sup>24</sup> Choi and co-workers also reported a high-concentration electrolyte that shows a high level of compatibility with Na<sub>4</sub>Fe<sub>3</sub>(PO<sub>4</sub>)<sub>2</sub>(P<sub>2</sub>O<sub>7</sub>) and Na<sub>0.7</sub>(Fe<sub>0.5</sub>Mn<sub>0.5</sub>)O<sub>2</sub> cathodes (>4.2 V vs Na/Na<sup>+</sup>) under high voltage and significantly reduces corrosion of metallic Na and aluminum current collectors in Na||stainless steel (SS) cells.<sup>25</sup> However, the high cost of salts, high viscosity of electrolytes, and poor wettability of the separators limit the application of high-concentration electrolytes. One effective way to address these drawbacks is to introduce an “inert” diluent to dilute HCEs, forming a localized high-concentration electrolyte (LHCE). This inert diluent dissolves in the solvent, while sodium salts are almost insoluble. When reducing the salt content and enhancing the electrolyte’s wetting properties, it is feasible to attain high levels of AGG and CIP.<sup>26</sup> Additionally, the diluent’s synergistic decomposition fosters the creation of a more reliable SEI. These factors collectively ensure higher Coulombic efficiency and enhanced cycling performance for SMBs.

In this work (perfluorobutoxy)methane (MTE) was introduced as the “inert” diluent into the HCE configured with NaFSI and DME, successfully preparing LHCE. As shown in Figure 1, in the presence of MTE, the coordination structure of Na<sup>+</sup> with anions in the high-concentration electrolyte is essentially retained. Notably, the MD simulation study indicates that MTE can decompose on the surface of metallic Na. Therefore, the coordination effect of solvation structure in LHCE and the synergistic action of MTE decomposition promotes the creation of an inorganic-enriched SEI. Electrochemical study discloses the average Coulombic efficiency of Na||Cu batteries can reach 98.3%, while the Na||Na-Fe<sub>1/3</sub>Ni<sub>1/3</sub>Mn<sub>1/3</sub>O<sub>2</sub> battery retains 86.4% capacity after 750 cycles at 1C. Consequently, Na||Na<sub>3</sub>V<sub>2</sub>(PO<sub>4</sub>)<sub>3</sub> can stably cycle at 1C, achieving an average Coulombic efficiency of 99.97% over 6200 cycles (approximately 517 days) with a capacity retention of 95.4%. Our study proposes a novel avenue to improve the stability and Coulombic efficiency of the SMB system which could also help for practical application in the future.

**Solvation Structure Analysis.** Three types of electrolytes were prepared to gain insight into the coordination behavior of Na<sup>+</sup> through Raman spectroscopy—dilute electrolyte (DE, NaFSI:DME = 1:9.8, molar ratio), high-concentration electrolyte (NaFSI:DME = 1:1.8, molar ratio), and localized high concentration electrolyte (NaFSI:DME:MTE = 1:1.8:1.1, molar ratio). As shown in Figure 2a, in DE, unbound DME displays two vibrational bands in the vicinity of 823 and 850 cm<sup>-1</sup>. However, these peaks are nearly undetectable in HCEs, suggesting an increased presence of unbound DME in DE and a reduction in the amount of free DME due to the addition of more NaFSI salt in HCE.<sup>27</sup> Besides, compared to DE, the peak of Na<sup>+</sup> coordinated DME (863 cm<sup>-1</sup>) is relatively lower in HCE, especially in LHCE, and this indicates the reduction in the amount of Na<sup>+</sup> coordinated DME in HCE and LHCE,

while in DE, the DME molecules take the helm in the solvation configuration. The bands appearing within the range 720–755 cm<sup>-1</sup> are caused by differently coordinated FSI<sup>-</sup>, as shown in Figure 2b.<sup>28</sup> Among the samples of three electrolytes, DE presents a solvation structure that includes solvent-separated ion pairs (SSIP) of 67% and contact ion pairs (CIP) of 33%, as shown in Figure 2c. With a rise in the salt concentration present in HCE, the proportion of free FSI<sup>-</sup> decreases to 22%, while the proportions of CIP and AGG rise to 44% and 34%, respectively.<sup>29–32</sup> After the addition of the diluent MTE, the free FSI<sup>-</sup> disappears and is replaced by a noticeable increase in the proportion of AGG structure. This indicates that although MTE does not participate in the solvation structure, its addition has forced more FSI<sup>-</sup> into the solvation shell, resulting in solvent-cation–anion aggregates within LHCE, as illustrated by the Molecular Dynamics (MD) simulation captured in Figure S1.

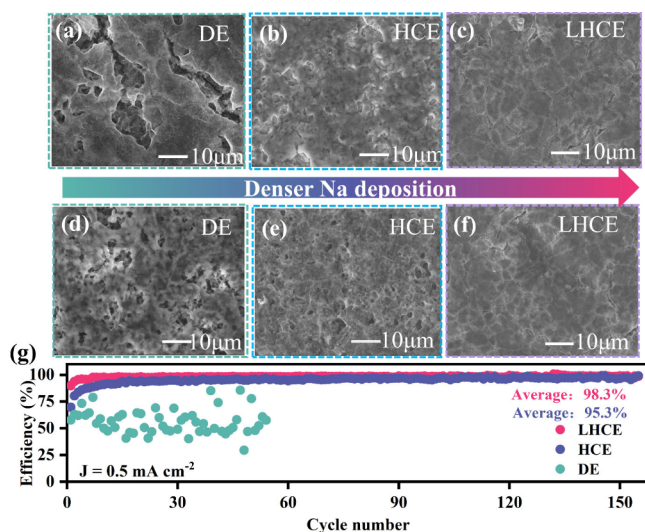
Further comprehension of the solvation structure of Na<sup>+</sup> in various types of electrolytes was provided through molecular dynamics simulations. The radial distribution functions obtained from MD simulations were analyzed for the coordination situation of Na<sup>+</sup> in the trio of electrolytes. As shown in Figure 2d–f, the peaks at 2.2 Å are attributed to Na-ODME and Na-OFSI pairs in all three electrolytes. Within DE, Na<sup>+</sup> are chiefly surrounded by the solvent molecules, while in HCE and LHCE, the coordination number of Na-OFSI pairs is higher, indicating that a good deal of FSI<sup>-</sup> have replaced solvent molecules in the inner solvation sheath of Na<sup>+</sup>. Furthermore, within LHCE, the notable increase in the peak intensity for Na-OFSI pairs denotes a more potent interaction between Na<sup>+</sup> and FSI<sup>-</sup>. Meanwhile, no obvious peak for Na-OMTE was observed in LHCE, indicating that MTE is hardly involved in the solvation structure of Na<sup>+</sup>.<sup>33</sup>

Figure 2g–i illustrates the interaction of Na<sup>+</sup> with FSI<sup>-</sup> and solvents such as DME or MTE across DE, HCE, and LHCE environments. Within DE, the primary solvation structure around Na<sup>+</sup> is primarily with DME, while the inner sheaths of the other two electrolytes are composed of DME and FSI<sup>-</sup>. In LHCE, after the addition of MTE, the interval separating Na<sup>+</sup> from FSI<sup>-</sup> contracts from 2.381 Å in HCE to 2.183 Å, signifying an intensified interaction. Meanwhile, in LHCE, the distance between Na<sup>+</sup> and DME increases from 2.249 Å in HCE to 2.343 Å, indicating a weakened interaction force between Na<sup>+</sup> and DME. Moreover, the distance between MTE and Na<sup>+</sup> is 5.516 Å, indicating that MTE stays out of the inner solvation shell. The remarkable congruence between MD simulations and Raman spectroscopy data underscores the practicality and dependability of introducing MTE diluent, which optimizes the solvation structure.

The stability of an electrolyte’s electrochemical kinetics is essential for maintaining a consistent electrode/electrolyte interface. Utilizing density functional theory (DFT) of quantum mechanics, we have determined the energy levels of the frontier molecular orbitals within the electrolyte’s chemical structure (Figure S2). DME and MTE possess higher LUMO levels than NaFSI, suggesting a lesser likelihood of decomposing prior to NaFSI. The predominant DME-Na-DME assembly in DE shows a higher LUMO level than the DME-Na-FSI assembly in HCE and LHCE, indicating that DME is more easily decomposed in DE. Furthermore, the decomposition process of MTE on the surface of sodium metal is observed (Figure S3). The decomposition of MTE produces more F atoms that combine with Na atoms, further increasing

the content of NaF formed on the surface of metallic Na.<sup>34</sup> This dynamic decomposition process can also be observed in [Video S1](#). In summary, the structure of the DME-Na-FSI that is generated in both HCE and LHCE is more favorable for the decomposition of NaFSI, and under the synergistic action of MTE decomposition, the SEI inorganic rich anion-derived SEI is easily generated on the surface of metallic Na, which provides good protection for the Na metal anode.

**Sodium Plating/Stripping Reversibility and SEI Properties.** The Coulombic efficiency of Na metal deposition/stripping in Na||Cu batteries with three electrolytes DE, HCE, and LHCE was studied, as shown in [Figure 2g](#). The surface morphology of Na metal in the Na||Cu batteries after 40 h of cycling with the three electrolytes at  $0.5 \text{ mA cm}^{-2}$  was observed by scanning electron microscopy (SEM), as shown in [Figure 3a–c](#). At low concentrations, Na||Cu batteries exhibit



**Figure 3.** SEM images of the Na anode surface using (a) DE, (b) HCE, and (c) LHCE after 40 h of cycling at  $0.5 \text{ mA cm}^{-2}$  for  $1 \text{ mAh cm}^{-2}$ . (d–f) SEM images of Na deposited on Cu electrodes at  $0.5 \text{ mA cm}^{-2}$  for  $1 \text{ mAh cm}^{-2}$  using (d) DE, (e) HCE, and (f) LHCE. (g) Cycling of the sodium metal CE in Na||Cu batteries using different electrolytes at  $0.5 \text{ mA cm}^{-2}$  and  $1.0 \text{ mAh cm}^{-2}$ .

low and unstable Coulombic efficiency; this occurs due to the reaction between a substantial quantity of unbound solvent molecules in the diluted electrolyte and the metallic Na, leading to erosive parasitic reactions as shown in [Figure 2a](#). Moreover, since most of the molecules coordinated with  $\text{Na}^+$  are solvent molecules, the SEI rich in inorganics derived from anions cannot be formed on the metallic sodium surface, failing to ensure reliable protection of the metallic Na anode and leading to the failure of Na||Cu batteries using DE after less than 60 cycles. The performance of Na||Cu batteries with HCE, which increases salt concentration, is greatly improved. The notably diminished quantity of unbound solvent molecules coupled with the greater quantity of anions in the  $\text{Na}^+$  coordination shell contributes to superior safeguarding of the sodium metal as shown in [Figure 3b](#), significantly improving the average Coulombic efficiency of Na||Cu batteries to a stable 95.3%. After diluting the salt concentration with MTE, the LHCE, with its good local concentrated solvation structure and the synergistic action of MTE decomposition, results in a smoother and flatter Na metal surface with a negligible presence of Na dendrites, showing

stability similar to that of HCE and even better Coulombic efficiency, with the first cycle Coulombic efficiency increased to 89% and an average Coulombic efficiency of 98.3% over 150 cycles, higher than those of HCE.

The uniformity of sodium Na is considered a pivotal parameter for the electrolyte-induced formation of the SEI. SEM was utilized to assess the surface contours of Na and the depth of Na deposits on the copper current collector. As shown in [Figure 3d](#), the deposition of Na is nonuniform, with a large exposed area of the electrolyte, presenting a rough, porous deposition morphology, which leads to unfavorable interfacial side reactions and accumulation of SEI, extremely detrimental to the long-term cycling of the battery. In the HCE, the previously observed uneven deposition has been markedly ameliorated. However, as shown in [Figure 3e](#), a certain degree of porosity and nonuniformity in the morphology persists. Notably, LHCE has resulted in a substantial enhancement in the density, uniformity, and smoothness of the deposited Na metal as shown in [Figure 3f](#). Additionally, the Na deposition layer of  $16 \mu\text{m}$  in thickness within the LHCE at a capacity of  $1 \text{ mAh cm}^{-2}$ , significantly thinner in comparison to the layers depicted in [Figure S4](#) for DE ( $43 \mu\text{m}$ ) and HCE ( $39 \mu\text{m}$ ). Besides, it can be observed from the side that the sodium deposition using LHCE is more compact compared to the loose and porous appearance after using DE and HCE. This refined microstructure is instrumental in providing enhanced protection for the Na metal anode, thereby fostering the long-term stability and cyclic performance of the battery.

The Tafel diagram facilitates the assessment of ion migration dynamics at the sodium-electrolyte interface across various electrolyte. From the Tafel plot of Na||Na batteries in HCE and LHCE ([Figure S5](#)), compared to the lower exchange current density of  $2.42 \text{ mA cm}^{-2}$  in HCE, the LHCE has a larger exchange current density of  $5.47 \text{ mA cm}^{-2}$ , indicating faster interfacial kinetics. Na||Na symmetric batteries are commonly used to evaluate the ability of electrolytes to protect Na metal anodes. [Figure S6](#) and [Figure S7](#) show the performance of Na||Na batteries, when cycled with electrolytes DE, HCE, and LHCE, examined at a current density rate of  $0.5 \text{ mA cm}^{-2}$ . The inherent incompatibility of DE with Na metal results in compromised cycling capability. Besides, batteries with HCE also exhibit terrible cycling stability and elevated overpotential. This shows that there are still serious side reactions and unstable SEI in HCE. Na||Na batteries employing LHCE demonstrate a remarkable cycling performance of up to 1350 h in contrast to the dramatic polarization growth after 250 h in the batteries with HCE electrolyte. Good cycling performance and voltage stability further indicate that dendrite growth is suppressed and the creation of a reliable SEI is achieved.

**Characteristics of SEI Films.** X-ray photoelectron spectroscopy (XPS) was utilized to evaluate the constituents of the SEI that form on cycled sodium metal. The XPS spectra of Na||Na batteries cycled for 40 h with three different electrolytes, namely DE, HCE, and LHCE, are presented in [Figure 4a,b](#). In [Figure 4a](#), the C 1s spectrum exhibits a stronger peak for DE, indicating that the SEI in the DE electrolyte is predominantly made up of organic substances that result from the DME solvent's decomposition. In contrast, the weaker C peak observed in both HCE and LHCE suggests less solvent molecule decomposition and the  $\text{FSI}^-$  anions are more actively involved in the SEI construction on the metallic Na surface,

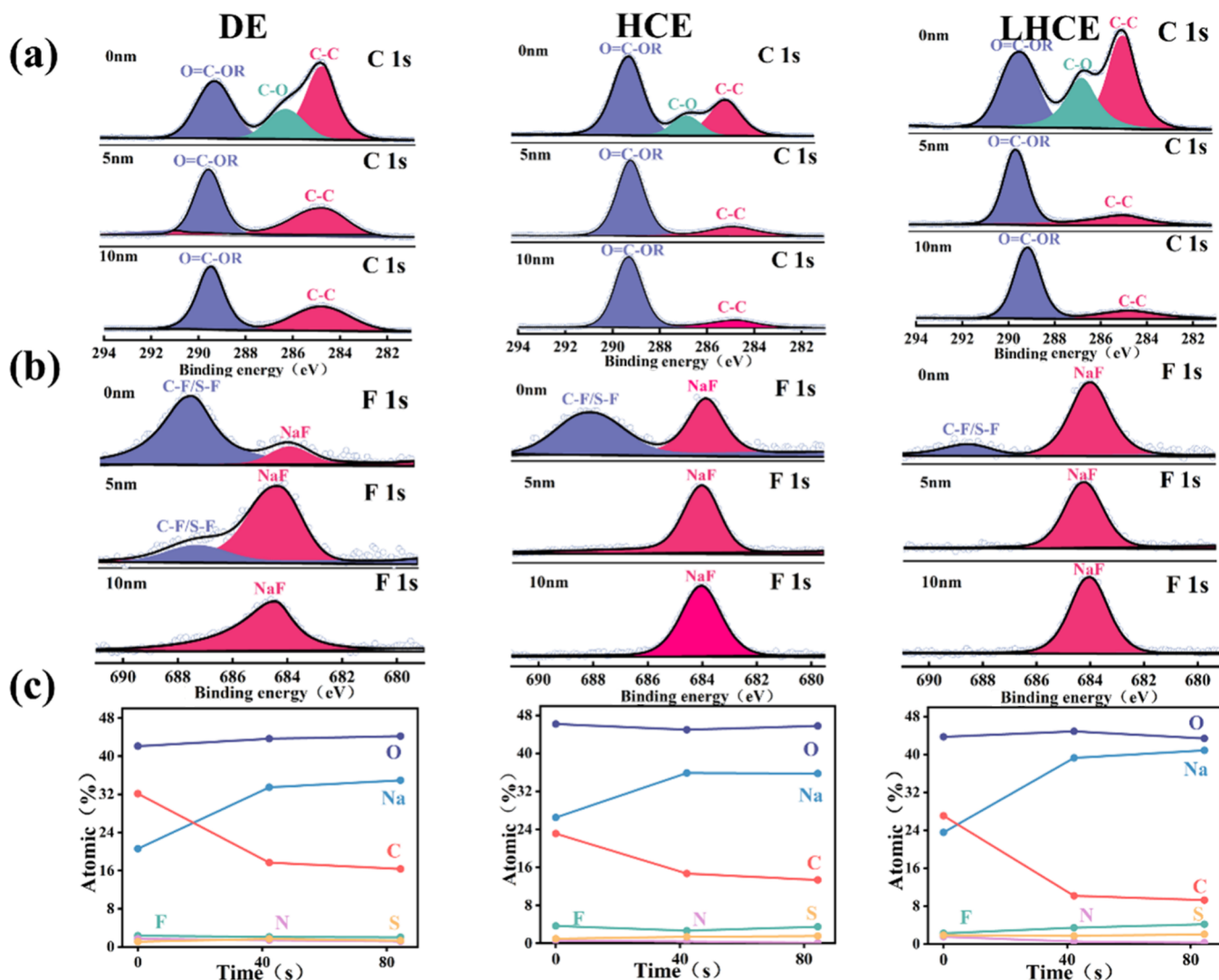


**Figure 4.** (a,b) XPS spectra of C 1s, F 1s with Ar<sup>+</sup> sputtering for 0, 5, and 10 nm. (c) Variations of elemental distributions in the SEI layers at different etching times.

which is further verified by the more pronounced NaF peak demonstrated in Figure 4b. Additionally, the O 1s spectrum (Figure S8b) reveals the presence of S=O groups in the SEI formed in LHCE, providing further evidence that the SEI contains decomposition products of FSI<sup>-</sup> anions, which are more stable than the organic products (C-O, C=O) formed in DE and HCE. Moreover, the presence of a significant amount of dense inorganic components such as NaO<sub>2</sub> and Na<sub>2</sub>CO<sub>3</sub> effectively shields the Na metal from direct contact with the electrolyte, enhancing the stability of the interfacial structure.<sup>35</sup> Furthermore, the S 2p spectrum (Figure S9) exhibits the peak of the inorganic component Na<sub>2</sub>S in LHCE but not in HCE and DE, suggesting that anion-induced decomposition enhancement facilitates the decomposition of FSI<sup>-</sup> on the surface of sodium metal. Additionally, the C-F/S-F peak in the F 1s spectrum also shows that the decomposition of FSI<sup>-</sup> in HCE and DE is insufficient, highlighting the unique role of LHCE in promoting FSI<sup>-</sup> decomposition.<sup>36</sup> Figure 4c and Figure S10 illustrate the variations in elemental distributions within the SEI layers at different etching times. Notably, after two sputtering processes, a gradual increase in Na content is observed in LHCE, surpassing that in DE and HCE. This suggests that the SEI

created on the surface of sodium metal after employing LHCE is thinner, which is more conducive to Na<sup>+</sup> transport. In summary, the inorganic-rich, dense, and thin SEI formed under the influence of LHCE is more beneficial for the protection of metal Na, reducing side reactions between the electrolyte and the Na metal, effectively suppressing the growth of Na dendrites and ensuring the long-term cycling stability of the battery.

**Electrochemical Performance.** To assess the viability of employing LHCE in practical batteries, we prepared coin batteries with Na<sub>3</sub>V<sub>2</sub>(PO<sub>4</sub>)<sub>3</sub> (NVP) and NaFe<sub>1/3</sub>Ni<sub>1/3</sub>Mn<sub>1/3</sub>O<sub>2</sub> (NFM) cathodes and Na metal anodes using three different electrolytes, BL (NaClO<sub>4</sub> in PC with 5% FEC in volume), HCE, and LHCE, to assess their electrochemical performance. Assembled Na||Al batteries were employed to investigate the oxidative stability of the electrolytes by using LSV (Figure S11). The LHCE containing MTE demonstrated superior oxidative stability. Consequently, Na||NFM batteries utilizing LHCE exhibited excellent cycling stability within a voltage range of 2.3–4 V. At a current density of 1C, the battery retained 86.4% of its capacity after 750 cycles. Compared to the BL, which experienced rapid capacity decay to 80%, and the HCE, which showed a continuous decline in Coulombic

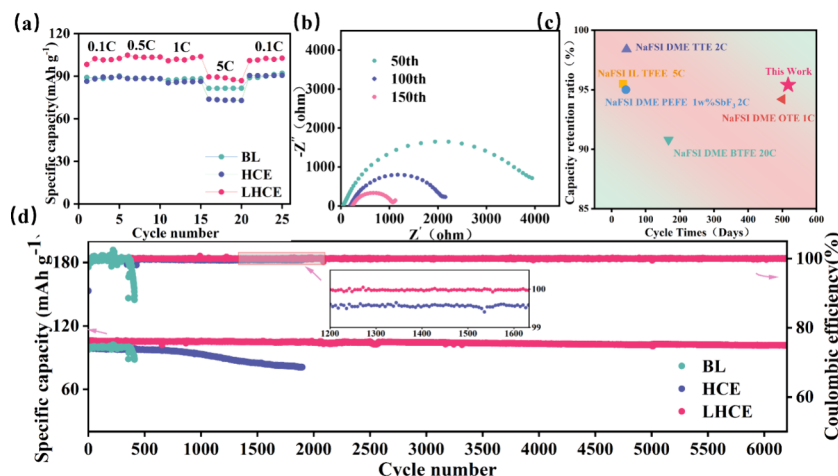


**Figure 5.** (a) Rate capability of Na||NVP batteries from 0.1C to 5C. (b) Nyquist plots of Na||NVP batteries using LHCE at the 50th, 100th and 150th cycles. (c) Comparison of cycle performance of various local high concentration electrolytes applied in Na||NVP batteries. (d) Cycling performance of Na||NVP batteries at 1C.

efficiency, the LHCE demonstrated better compatibility with the Na||NFM battery. As observed in Figure 5a, the rate performance of NVP batteries shows that the battery with LHCE, compared to the other two electrolytes, exhibits a negligible decrease in capacity even when the current is ramped up from 0.1C to 1C, which indicates the good rate capability. The ion-transport kinetics in the HCE and LHCE is further investigated by electrochemical impedance spectroscopy (EIS) analysis (Figure S14); the LHCE exhibits a higher ionic conductivity, which is attributed to the reduction in the viscosity of the electrolyte. As shown in Figure 5b, the Nyquist plots of Na||NVP batteries using LHCE at the 50th, 100th, and 150th cycles indicate that the impedance gradually decreases after the 50th–150th cycles, suggesting the formation of a SEI with low surface resistance in the battery, which is beneficial for the deposition of sodium ions and long-term cycling of the battery. All of the above can be verified through Figure 5d, which compares the long cycling performance of Na||NVP batteries with the three electrolytes in the voltage range of 2.5–3.8 V. The battery with BL electrolyte shows a rapid capacity decay to battery failure at 410 cycles. However, the battery with HCE can stably cycle to 1900 cycles, at which point the capacity decays to 80%. In contrast, the battery with LHCE exhibits even better cycling performance, with a capacity retention of 95.4% after 6200 cycles (about 517 days), and an average Coulombic efficiency of over 99.9%, up to 99.97%, which is much higher than the 99.29% of the battery with BL electrolyte and the 99.67% of the battery with HCE. In summary, compared with detailed electrochemical data from other studies (Table S1), our work demonstrates outstanding performance especially in the long cycle life of the Na||NVP battery from Figure 5c.<sup>22,34–37</sup>

In summary, this work reports on the design of an electrolyte that provides effective protection for metallic sodium anodes, achieving ultralong cycling performance and high Coulombic efficiency in sodium metal batteries. By introducing MTE as a diluent in the HCE, the original solvation frameworks of CIPs and AGGs within HCE are sustained, while enhancing the interaction between Na<sup>+</sup> and FSI<sup>-</sup>. Additionally, the synergistic decomposition of MTE contributes to the creation of a more reliable and robust SEI on the surface of the Na anode. This is reflected in the Na||NaFe<sub>1/3</sub>Ni<sub>1/3</sub>Mn<sub>1/3</sub>O<sub>2</sub> battery retaining

86.4% capacity after 750 cycles at 1C and the Na||NVP batteries maintaining a capacity retention of 95.4% and an Coulombic efficiency of 99.97% after 517 days of cycling at 1C. The stability of cycling performance and the Coulombic efficiency are critical metrics for evaluating energy storage in batteries. Consequently, this work offers valuable insights into the preservation of the Na anode, which is essential for the development of high-performing and durable sodium metal batteries.

## ASSOCIATED CONTENT

### Supporting Information

The Supporting Information is available free of charge at <https://pubs.acs.org/doi/10.1021/acsenergylett.4c02751>.

Details of the experimental procedures, materials used, and test methods, MD simulations, SEM images, additional electrochemical data, XPS data, and comparison of the levels of our materials with those reported ([PDF](#))

Video S1, dynamic decomposition of MTE on sodium metal ([MP4](#))

## AUTHOR INFORMATION

### Corresponding Authors

Min Jia – School of Material Science and Engineering, Jiangsu University, Zhenjiang 212013, P. R. China; Email: [mjia@ujs.edu.cn](mailto:mjia@ujs.edu.cn)

Xiaoyu Zhang – School of Material Science and Engineering, Jiangsu University, Zhenjiang 212013, P. R. China; [orcid.org/0000-0002-4336-2250](https://orcid.org/0000-0002-4336-2250); Email: [x.zhang@ujs.edu.cn](mailto:x.zhang@ujs.edu.cn)

Haoshen Zhou – Center of Energy Storage Materials & Technology, College of Engineering and Applied Sciences, Jiangsu Key Laboratory of Artificial Functional Materials, National Laboratory of Solid State Micro-structures, and Collaborative Innovation Center of Advanced Micro-structures, Nanjing University, Nanjing 210093, P. R. China; [orcid.org/0000-0001-8112-3739](https://orcid.org/0000-0001-8112-3739); Email: [hszhou@nju.edu.cn](mailto:hszhou@nju.edu.cn)

**Authors**

Zhangbin Cheng – School of Material Science and Engineering, Jiangsu University, Zhenjiang 212013, P. R. China

Zehui Zhang – Center of Energy Storage Materials & Technology, College of Engineering and Applied Sciences, Jiangsu Key Laboratory of Artificial Functional Materials, National Laboratory of Solid State Micro-structures, and Collaborative Innovation Center of Advanced Micro-structures, Nanjing University, Nanjing 210093, P. R. China

Feilong Qiu – School of Integrated Circuits, East China Normal University, Shanghai 200241, P. R. China

Zheng Gao – School of Material Science and Engineering, Jiangsu University, Zhenjiang 212013, P. R. China

Haijiao Xie – Hangzhou Yanqu Information Technology Co., Ltd, Hangzhou City, Zhejiang Province 310003, P. R. China

Zhen Xu – School of Chemistry and Chemical Engineering, Qilu University of Technology (Shandong Academy of Sciences), Jinan 250353, P. R. China

Complete contact information is available at:

<https://pubs.acs.org/10.1021/acsenergylett.4c02751>

**Notes**

The authors declare no competing financial interest.

**ACKNOWLEDGMENTS**

This work was supported by the National Natural Science Foundation of China (nos. 22005138, 52072154, 12174158) and Jiangsu Province Carbon Peak and Neutrality Innovation Program (Industry tackling on prospect and key technology) BE2022002-2.

**REFERENCES**

- (1) Oh, S. M.; Myung, S. T.; Yoon, C. S.; Lu, J.; Hassoun, J.; Scrosati, B.; Amine, K.; Sun, Y. K. Advanced Na[Ni<sub>0.25</sub>Fe<sub>0.5</sub>Mn<sub>0.25</sub>]O<sub>2</sub>/C-Fe<sub>3</sub>O<sub>4</sub> Sodium-Ion Batteries Using EMS Electrolyte for Energy Storage. *Nano Lett.* **2014**, *14* (3), 1620–1626.
- (2) Yao, N.; Chen, X.; Fu, Z. H.; Zhang, Q. Applying Classical, Ab Initio, and Machine-Learning Molecular Dynamics Simulations to the Liquid Electrolyte for Rechargeable Batteries. *Chem. Rev.* **2022**, *122* (12), 10970–11021.
- (3) Shi, H.; Zhang, Y.; Liu, Y.; Yuan, C. Metallic Sodium Anodes for Advanced Sodium Metal Batteries: Progress, Challenges and Perspective. *Chem. Rec.* **2022**, *22* (10), No. e202200112.
- (4) Lee, B.; Paek, E.; Mitlin, D.; Lee, S. W. Sodium Metal Anodes: Emerging Solutions to Dendrite Growth. *Chem. Rev.* **2019**, *119* (8), 5416–5460.
- (5) Zhao, C.; Wang, Q.; Yao, Z.; Wang, J.; Sánchez-Lengeling, B.; Ding, F.; Qi, X.; Lu, Y.; Bai, X.; Li, B. J. S.; et al. Rational design of layered oxide materials for sodium-ion batteries. *Science* **2020**, *370* (6517), 708–711.
- (6) Zheng, Q.; Yamada, Y.; Shang, R.; Ko, S.; Yamada, A.; et al. A cyclic phosphate-based battery electrolyte for high voltage and safe operation. *Nature Energy* **2020**, *5* (4), 291–298.
- (7) Chen, S.; Zheng, J.; Yu, L.; Ren, X.; Engelhard, M. H.; Niu, C.; Lee, H.; Xu, W.; Xiao, J.; Liu, J.; Zhang, J.-G. High-Efficiency Lithium Metal Batteries with Fire-Retardant Electrolytes. *Joule* **2018**, *2* (8), 1548–1558.
- (8) Yoon, H.; Zhu, H.; Hervault, A.; Armand, M.; MacFarlane, D. R.; Forsyth, M. Physicochemical properties of N-propyl-N-methyl-pyrrolidinium bis(fluorosulfonyl)imide for sodium metal battery applications. *Phys. Chem. Chem. Phys.* **2014**, *16* (24), 12350–12355.
- (9) Mohd Noor, S. A.; Yoon, H.; Forsyth, M.; MacFarlane, D. R. Gelled ionic liquid sodium ion conductors for sodium batteries. *Electrochim. Acta* **2015**, *169*, 376–381.
- (10) Chen, J.; Fan, X.; Li, Q.; Yang, H.; Khoshi, M. R.; Xu, Y.; Hwang, S.; Chen, L.; Ji, X.; Yang, C.; He, H.; Wang, C.; Garfunkel, E.; Su, D.; Borodin, O.; Wang, C. Electrolyte design for LiF-rich solid-electrolyte interfaces to enable high-performance microsized alloy anodes for batteries. *Nature Energy* **2020**, *5* (5), 386–397.
- (11) Wang, S.; Jiang, Y.; Hu, X. Ionogel-Based Membranes for Safe Lithium/Sodium Batteries. *Adv. Mater.* **2022**, *34* (52), 2200945.
- (12) Manthiram, A.; Yu, X. Ambient Temperature Sodium-Sulfur Batteries. *Small* **2015**, *11* (18), 2108–2114.
- (13) Hartmann, P.; Bender, C. L.; Vraca, M.; Durr, A. K.; Garsuch, A.; Janek, J.; Adelhelm, P. A rechargeable room-temperature sodium superoxide (NaO<sub>2</sub>) battery. *Nat. Mater.* **2013**, *12* (3), 228–32.
- (14) Hu, X.; Li, Z.; Chen, J. Flexible Li-CO<sub>(2)</sub> Batteries with Liquid-Free Electrolyte. *Angew. Chem., Int. Ed. Engl.* **2017**, *56* (21), 5785–5789.
- (15) Lutz, L.; Alves Dalla Corte, D.; Tang, M.; Salager, E.; Deschamps, M.; Grimaud, A.; Johnson, L.; Bruce, P. G.; Tarascon, J.-M. Role of Electrolyte Anions in the Na-O<sub>2</sub> Battery: Implications for NaO<sub>2</sub> Solvation and the Stability of the Sodium Solid Electrolyte Interphase in Glyme Ethers. *Chem. Mater.* **2017**, *29* (14), 6066–6075.
- (16) Tian, Y.; Zeng, G.; Rutt, A.; Shi, T.; Kim, H.; Wang, J.; Koettgen, J.; Sun, Y.; Ouyang, B.; Chen, T.; Lun, Z.; Rong, Z.; Persson, K.; Ceder, G. Promises and Challenges of Next-Generation "Beyond Li-ion" Batteries for Electric Vehicles and Grid Decarbonization. *Chem. Rev.* **2021**, *121* (3), 1623–1669.
- (17) Yabuuchi, N.; Kubota, K.; Dahbi, M.; Komaba, S. Research Development on Sodium-Ion Batteries. *Chem. Rev.* **2014**, *114* (23), 11636–11682.
- (18) Wang, Z.; Qi, F.; Yin, L.; Shi, Y.; Sun, C.; An, B.; Cheng, H.-M.; Li, F. An Anion-Tuned Solid Electrolyte Interphase with Fast Ion Transfer Kinetics for Stable Lithium Anodes. *Adv. Energy Mater.* **2020**, *10* (14), 1903843.
- (19) Yang, Z.; He, J.; Lai, W. H.; Peng, J.; Liu, X. H.; He, X. X.; Guo, X. F.; Li, L.; Qiao, Y.; Ma, J. M. Fire-Retardant, Stable-Cycling and High-Safety Sodium Ion Battery. *Angew. Chem.* **2021**, *60* (52), 27086–27094.
- (20) Yamada, Y.; Wang, J.; Ko, S.; Watanabe, E.; Yamada, A. Advances and issues in developing salt-concentrated battery electrolytes. *Nature Energy* **2019**, *4* (4), 269–280.
- (21) Yamada, Y.; Furukawa, K.; Sodeyama, K.; Kikuchi, K.; Yaegashi, M.; Tateyama, Y.; Yamada, A. Unusual Stability of Acetonitrile-Based Superconcentrated Electrolytes for Fast-Charging Lithium-Ion Batteries. *J. Am. Chem. Soc.* **2014**, *136* (13), 5039–5046.
- (22) Zheng, J.; Chen, S.; Zhao, W.; Song, J.; Engelhard, M. H.; Zhang, J.-G. Extremely Stable Sodium Metal Batteries Enabled by Localized High-Concentration Electrolytes. *Acs Energy Letters* **2018**, *3* (2), 315–321.
- (23) Kim, M.; An, J.; Shin, S.-J.; Hwang, I.; Lee, J.; Park, Y.; Kim, J.; Park, E.; Kim, J.; Park, G.; Kim, S.; Coskun, A.; Choi, J. W. Anti-corrosive electrolyte design for extending the calendar life of lithium metal batteries. *Energy Environ. Sci.* **2024**, *17* (16), 6079–6090.
- (24) Cao, R.; Mishra, K.; Li, X.; Qian, J.; Engelhard, M. H.; Bowden, M. E.; Han, K. S.; Mueller, K. T.; Henderson, W. A.; Zhang, J.-G. Enabling room temperature sodium metal batteries. *Nano Energy* **2016**, *30*, 825–830.
- (25) Lee, J.; Lee, Y.; Lee, J.; Lee, S.-M.; Choi, J.-H.; Kim, H.; Kwon, M.-S.; Kang, K.; Lee, K. T.; Choi, N.-S. Ultraconcentrated Sodium Bis(fluorosulfonyl)imide-Based Electrolytes for High-Performance Sodium Metal Batteries. *ACS Appl. Mater. Interfaces* **2017**, *9* (4), 3723–3732.
- (26) Yang, M. Y.; Zybin, S. V.; Das, T.; Merinov, B. V.; Goddard, W. A., III; Mok, E. K.; Hah, H. J.; Han, H. E.; Choi, Y. C.; Kim, S. H. Characterization of the Solid Electrolyte Interphase at the Li Metal-Ionic Liquid Interface. *Adv. Energy Mater.* **2023**, *13* (3), 2202949.
- (27) Qin, L.; Xiao, N.; Zheng, J.; Lei, Y.; Zhai, D.; Wu, Y. Localized High-Concentration Electrolytes Boost Potassium Storage in High-Loading Graphite. *Adv. Energy Mater.* **2019**, *9* (44), 1902618.
- (28) Zhao, Y.; Zhou, T.; Mensi, M.; Choi, J. W.; Coskun, A. Electrolyte engineering via ether solvent fluorination for developing

stable non-aqueous lithium metal batteries. *Nat. Commun.* **2023**, *14* (1), 299.

(29) Ren, X.; Chen, S.; Lee, H.; Mei, D.; Engelhard, M. H.; Burton, S. D.; Zhao, W.; Zheng, J.; Li, Q.; Ding, M. S.; Schroeder, M.; Alvarado, J.; Xu, K.; Meng, Y. S.; Liu, J.; Zhang, J.-G.; Xu, W. Localized High-Concentration Sulfone Electrolytes for High-Efficiency Lithium-Metal Batteries. *Chem.* **2018**, *4* (8), 1877–1892.

(30) Kim, J.; Koo, B.; Lim, J.; Jeon, J.; Lim, C.; Lee, H.; Kwak, K.; Cho, M. Dynamic Water Promotes Lithium-Ion Transport in Superconcentrated and Eutectic Aqueous Electrolytes. *AcS Energy Letters* **2022**, *7* (1), 189–196.

(31) Wen, Z.; Fang, W.; Wu, X.; Qin, Z.; Kang, H.; Chen, L.; Zhang, N.; Liu, X.; Chen, G. High-Concentration Additive and Triiodide/Iodide Redox Couple Stabilize Lithium Metal Anode and Rejuvenate the Inactive Lithium in Carbonate-Based Electrolyte. *Adv. Funct. Mater.* **2022**, *32* (35), 2204768.

(32) Ding, J.-F.; Xu, R.; Yao, N.; Chen, X.; Xiao, Y.; Yao, Y.-X.; Yan, C.; Xie, J.; Huang, J.-Q. Non-Solvating and Low-Dielectricity Cosolvent for Anion-Derived Solid Electrolyte Interphases in Lithium Metal Batteries. *Angew. Chem., Int. Ed.* **2021**, *60* (20), 11442–11447.

(33) Zheng, X.; Huang, L.; Luo, W.; Wang, H.; Dai, Y.; Liu, X.; Wang, Z.; Zheng, H.; Huang, Y. Tailoring Electrolyte Solvation Chemistry toward an Inorganic-Rich Solid-Electrolyte Interphase at a Li Metal Anode. *AcS Energy Letters* **2021**, *6* (6), 2054–2063.

(34) Wang, Y.; Jiang, R.; Liu, Y.; Zheng, H.; Fang, W.; Liang, X.; Sun, Y.; Zhou, R.; Xiang, H. Enhanced Sodium Metal/Electrolyte Interface by a Localized High-Concentration Electrolyte for Sodium Metal Batteries: First-Principles Calculations and Experimental Studies. *AcS Applied Energy Materials* **2021**, *4* (7), 7376–7384.

(35) Liu, Y.; Lu, S.; Wang, Z.; Xu, J.; Weng, S.; Xue, J.; Tu, H.; Zhang, F.; Liu, L.; Gao, Y.; Li, H.; Zheng, J.; Wu, X. Weakly Polar Ether-Aided Ionic Liquid Electrolyte Enables High-Performance Sodium Metal Batteries over Wide Temperature Range. *Adv. Funct. Mater.* **2024**, *34* (28), 2312295.

(36) Zhou, X.; Zhang, Q.; Zhu, Z.; Cai, Y.; Li, H.; Li, F. Anion-Reinforced Solvation for a Gradient Inorganic-Rich Interphase Enables High-Rate and Stable Sodium Batteries. *Angew. Chem., Int. Ed.* **2022**, *61* (30), No. e202205045.

(37) Fang, W.; Jiang, R.; Zheng, H.; Zheng, Y.; Sun, Y.; Liang, X.; Xiang, H.-F.; Feng, Y.-Z.; Yu, Y. Stable sodium metal anode enhanced by advanced electrolytes with  $SbF_3$  additive. *Rare Metals* **2021**, *40* (2), 433–439.